Quantum phase transitions studied within the interacting boson model

Pavel Cejnar[1,*] and Jan Jolie[2,†]
[1]*Institute of Particle and Nuclear Physics, Charles University, V Holešovičkách 2, 180 00 Prague, Czech Republic*
[2]*Institute of Physics, University of Fribourg, Pérolles, 1700 Fribourg, Switzerland*
(Received 20 December 1999)

We study quasicritical phenomena in transitions between two ''quantum phases'' of a finite boson system, described by the interacting boson model 1 used in nuclear physics. The model is formulated in the algebraic framework and has a simple geometrical interpretation; the ''phases'' represented by dynamical symmetries U(5) and SU(3) correspond to spherical and deformed nuclear shapes. The quasicriticality of the U(5)-SU(3) transition is shown to be connected with the following phenomena simultaneously occurring in a narrow parameter region between the symmetries: (a) abrupt structural changes of eigenstates, (b) multiple avoided crossing of levels, (c) peaked density of exceptional points, (d) qualitative changes of the corresponding classical potential. We show that these spectroscopic features influence the dynamics of intersymmetry transitions in the model parameter space if the parameters themselves become dynamical variables.

PACS number(s): 05.70.Fh, 21.60.Fw

I. INTRODUCTION

Consider a Hamiltonian given by the following weighted sum of two incompatible parts:

$$\hat{H}_\lambda = (1-\lambda)\hat{H}_0 + \lambda \hat{H}_1, \quad \lambda \in [0,1]. \tag{1}$$

The terms $\hat{H}_0$ and $\hat{H}_1$ (with $[\hat{H}_0, \hat{H}_1] \neq 0$) may represent two fundamental modes of motion—suppose that they are classified by two different dynamical symmetries [1]—and $\hat{H}_\lambda$ is intermediate between them for $\lambda \in (0,1)$. Parameter λ thus controls the transition between both dynamical limits. Do the features of $\hat{H}_\lambda$ go smoothly from one limit to the other, or do they flip at a certain critical λ? The answer, of course, depends on what particular terms in Eq. (1) are considered. Although one somehow tends to expect a smooth change of properties, the critical, ''phase-transitional'' behavior is encountered in a number of physically relevant situations [2–8]. It is met in nuclear physics, for instance, where the $\hat{H}_0$ and $\hat{H}_1$ ''phases'' usually represent normal and superconducting or rotational and vibrational modes of the nuclear motion.

In this paper, the phenomenon of ''quantum phase transition,'' as we tentatively call it, is studied within a simple model that describes an ensemble of interacting bosons [9]. Our choice is motivated by the transparent algebraic structure of this model, but also by its relation to real atomic nuclei. The former ensures well defined dynamical symmetries and transitions between them controlled by a few model parameters. The latter follows from the fact that in an appropriate coordinate representation the bosonic Hamiltonian turns out to describe certain rotational and vibrational motions of a ''quantum drop,'' i.e., images nuclear collective degrees of freedom. In this sense, the model used is an elegant example, realistic and toy at the same time.

The phase transition that we will be dealing with is usually tracted as a transition between spherical and deformed nuclear shapes [6,7]. We will discuss both the spectroscopic and dynamical consequences of this transition—see Secs. III and IV. Here, the term ''spectroscopic'' is used for the phenomena directly related to wave functions and energies of the Hamiltonian eigenstates. It will be shown that the quantum phase transitions are characterized by quite specific changes of this kind, changes that take place in a very narrow parameter interval around the critical point. The term ''dynamical,'' on the other hand, is reserved for those phenomena that are encountered if the intersymmetry transition, the deformation in our case, is considered as a dynamical process. In such a case, the model parameters become dynamical variables coupled to an external physical system, and the qualitative changes of the Hamiltonian in the critical region influence their evolution.

In spite of the specific character of the model used we believe that our results hold qualitatively also for other quantum parameter-dependent Hamiltonians that exhibit critical behavior and will thus be valuable for understanding the quantum phase-transitional phenomena in general.

II. REVIEW OF THE MODEL

We will study the transitions in the parameter space of the simplest nuclear interacting boson model, commonly abbreviated as the IBM-1 [9,10]. This model describes a system of a fixed number (N) of spin=0 and 2 bosons (s and d bosons) subject to one- and two-body interactions. The IBM-1 reveals a transparent algebraic structure with U(6) as the dynamical group. Varying six free parameters of the model (this number results from plausible requirements set on the Hamiltonian), one can reach three standard dynamical symmetries—U(5), SU(3), and SO(6)—and two additional ones—SU(3)* and SO(6)* (differing from the corresponding standard symmetries only by gauge transformations of the boson operators) [9]. It turns out (see also below) that these dynamical symmetries provide an appropriate framework for the description of low-energy collective motions of real nu-

*Electronic address: pavel.cejnar@mff.cuni.cz
†Electronic address: jan.jolie@unifr.ch

clei with certain shape symmetries: (a) the U(5) limit corresponds to spherical nuclei, (b) the SU(3) and SU(3)* limits to axially symmetric nuclei with a quadrupole deformation [two SU(3) realizations distinguish prolate and oblate shapes [9]], and (c) the SO(6) and SO(6)* limits to quadrupolly deformed nuclei that are unstable against the axial-symmetry breaking [9] or even have tendency for a small stabilized triaxiality [11] (two SO(6) realizations differ in electric quadrupole properties [12]).

In this work we adopt a simplified, two-parameter IBM-1 Hamiltonian from Ref. [13]:

$$\hat{H}_{(\eta,\chi)}=(1-\eta)\left[-\frac{\hat{Q}_\chi\cdot\hat{Q}_\chi}{N}\right]+\eta\,\hat{n}_d,$$

$$\eta\in[0,1],\quad \chi\in[-\sqrt{7}/2,0]. \tag{2}$$

Here, $\hat{n}_d$ is the d-boson number operator and $\hat{Q}_\chi$ a quadrupole operator,

$$\hat{n}_d=d^\dagger\cdot\tilde{d}, \tag{3}$$

$$\hat{Q}_\chi=d^\dagger s+s^\dagger\tilde{d}+\chi[d^\dagger\times\tilde{d}]^{(2)}, \tag{4}$$

with $[d^\dagger\times\tilde{d}]^{(2)}$ standing for the $l=2$ tensor coupling of the d-boson creation and annihilation operators [$\tilde{d}_\mu=(-1)^\mu d_{-\mu}$, where $\mu=-2\ldots+2$ is the angular-momentum projection] and ''$\cdot$'' denoting the scalar product. While η and χ are varied as the control parameters, the total number of bosons N is taken as a constant. Clearly, $\hat{H}_{(\eta,\chi)}$ is of the form of $\hat{H}_\lambda$ from Sec. I if χ is constant. The (η,χ)-parameter sheet of Eq. (2) contains the standard IBM-1 dynamical symmetries: U(5) for $\eta=1$, SU(3) for $\eta=0$, $\chi=-\sqrt{7}/2$, and SO(6) for $\eta=\chi=0$. The nonstandard symmetries, on the other hand, are absent [14] (we choose here the phase convention from Ref. [10]). A natural representation of the parameter sheet is in a nonrectangular coordinate grid that maps the rectangle defined in Eq. (2) onto a triangle (the so-called Casten triangle [9]) with vertices corresponding to the standard dynamical symmetries and the other points to various transitional cases (see Fig. 7 below).

Since the model is analytically soluble in the dynamical-symmetry limits, the textbooks mostly deal with only these cases, the transitional Hamiltonians leaving just for a numerical treatment. One of the aims of this paper is to show that the intersymmetry transitions are not only more generic in nature than the exact symmetries, but also perhaps more interesting in some respect. An important feature studied in this connection is the onset of chaos in such transitions. The Hamiltonian (2) is exactly integrable in the symmetry limits and also along the SO(6)-U(5) leg of the Casten triangle ($\chi=0$), which leads to semiregular properties in neighboring parameter regions. No other case of integrability is known. The dynamics outside these nearly integrable regions was indeed found to be mostly chaotic—with one important exception, however. A narrow strip of increased regularity was found [13] in the parametrization represented by Eq. (2) along the $\chi\approx(\sqrt{7}-1)\eta/2-\sqrt{7}/2$ curve connecting the SU(3) and U(5) limits through the triangle interior. Thus the suppression of chaos is not a privilege of the regions close to integrable. Transitions between various dynamical symmetries can but may not lead through completely chaotic intermediate regimes. We must admit that the explanation for this behavior is still missing although recently some hint was given [14,15] by the analysis of wave-function entropies of the Hamiltonian eigenstates with respect to the symmetry bases.

Another interesting feature that can be investigated with the intersymmetry IBM-1 Hamiltonians is the above-mentioned critical behavior [6,7]. The model in the most general parametrization exhibits a phase transition with respect to the U(5)-symmetry breaking. It turns out that if the Hamiltonian with the U(5) dynamical symmetry is perturbed, the ground-state structure remains basically the U(5) structure until some critical perturbation is reached. At this point, the ground state flips to another form and continues varying slowly as the perturbation goes on.

More precisely, what the IBM experts call the shape-phase transition is standardly derived in the following way: The model ground state is considered within the mean-field approximation, i.e., in the form of the boson condensate $|N,\vec{\alpha}\rangle\propto(\alpha_s s^\dagger+\Sigma_\mu\alpha_\mu d^\dagger_\mu)^N|0\rangle$ (where $|0\rangle$ is the boson vacuum). Any such state can be expressed via an appropriate rotation of the ''intrinsic'' condensate state,

$$|N,\beta,\gamma\rangle\propto\left(s^\dagger+\beta\cos\gamma d^\dagger_0+\frac{\beta\sin\gamma}{\sqrt{2}}[d^\dagger_2+d^\dagger_{-2}]\right)^N|0\rangle, \tag{5}$$

where β and γ allow to be interpreted [16] as corresponding to the Bohr parameters of the intrinsic-frame quadrupole deformation in the drop model [Bohr geometrical parameters appear in the expansion $R(\theta,\phi)\propto1+\Sigma_\mu a_\mu Y_{2\mu}(\theta,\phi)$ of the nuclear surface if the coefficients a_μ are written in the same way as α_μ's in Eq. (5)]. The variational method is then applied to find the optimal values of these variables, i.e., the values that minimize the energy functional $E(N,\beta,\gamma)=\langle N,\beta,\gamma|\hat{H}|N,\beta,\gamma\rangle$. It turns out that if the U(5)-symmetry breaking reaches the critical point, the optimal value of β moves abruptly from zero [value corresponding to the U(5) symmetry] to nonzero. Within the above-mentioned geometrical interpretation this transition mimics the flip of the nuclear shape from spherical ($\beta=0$) to a prolate ($\beta>0$) form.

To be concrete, the Hamiltonian in Eq. (2) yields the energy functional as follows (cf. [16]):

$$\begin{aligned}E_{(\eta,\chi)}(N,\beta,\gamma)=&-5(1-\eta)+\frac{1}{(1+\beta^2)^2}\Bigg\{[N\eta-(1-\eta)\\&\times(4N+\chi^2-8)]\beta^2+\Bigg[N\eta-(1-\eta)\\&\times\left(\frac{2N+5}{7}\chi^2-4\right)\Bigg]\beta^4\\&+\left[4\sqrt{\frac{2}{7}}N(1-\eta)\chi\right]\beta^3\cos3\gamma\Bigg\}.\end{aligned} \tag{6}$$

The critical point in the above expression is given by the value of η where the coefficient at β^2 vanishes, i.e.,

$$\eta_N^c(\chi)=\frac{4N+\chi^2-8}{5N+\chi^2-8}. \tag{7}$$

At this value, the second β derivative of Eq. (6) for $\beta=0$ changes its sign, which means that the $\beta=0$ maximum becomes a local minimum. Note that the critical point (7) depends on χ: it changes between $\eta_N^c(-\sqrt{7}/2)=(16N-25)/(20N-25)$ at the SU(3)-U(5) side of the Casten triangle and $\eta_N^c(0)=(16N-32)/(20N-32)$ at the SO(6)-U(5) side, but this dependence is practically negligible for sufficiently large boson numbers (even with $N=10$ the critical region is located within a narrow interval between 0.762 and 0.771). It should be mentioned that a more sophisticated numerical treatment [11,22] with an angular-momentum projection of the state (5) would yield an energy functional and phase separatrix differing in general from those in Eqs. (6) and (7). Both these approaches, however, converge as N goes to infinity.

Another method used for studying the IBM phase transition is based on the time-dependent variational principle with the coherent state $|\vec{\alpha}\rangle\propto\exp(\alpha_s s^\dagger+\Sigma_\mu\alpha_\mu d_\mu^\dagger)|0\rangle$ trial functions [17,18]. For $N\to\infty$ this procedure yields the classical limit of the model. The classical IBM-1 Hamiltonian depends on five coordinates and associated momenta, $\mathcal{H}_{(\eta,\chi)}(q_i,p_i)$, while its potential-energy part $\mathcal{V}_{(\eta,\chi)}(q_i)\equiv\mathcal{H}_{(\eta,\chi)}(q_i,p_i=0)$ (classical potential) only on two appropriately chosen coordinates. In particular, for the Hamiltonian (2) we have

$$\mathcal{V}_{(\eta,\chi)}(\tilde{\beta},\tilde{\gamma})\propto\left[\frac{5}{2}\eta-2\right]\tilde{\beta}^2+\left[(1-\eta)\left(1-\frac{\chi^2}{14}\right)\right]\tilde{\beta}^4+\left[\frac{2}{\sqrt{7}}(1-\eta)\chi\right]\tilde{\beta}^3\sqrt{1-\frac{\tilde{\beta}^2}{2}}\cos 3\tilde{\gamma}, \tag{8}$$

where $\tilde{\beta}$ and $\tilde{\gamma}$ are connected with the above-defined intrinsic shape variables through the relation

$$\tilde{\beta}=\frac{\sqrt{2}\beta}{\sqrt{1+\beta^2}},\quad \tilde{\gamma}=\gamma, \tag{9}$$

which maps the restricted interval of $\tilde{\beta}\in[0,\sqrt{2}]$ onto the infinite range $\beta\in[0,\infty)$ in the standard parametrization [19]. It is easy to check that the potential $\mathcal{V}_{(\eta,\chi)}(\tilde{\beta},\tilde{\gamma})$ with the substitution (9) is nothing but the $N\to\infty$ limit of $E_{(\eta,\chi)}(N,\beta,\gamma)/N$. Both expressions (8) and (6) are thus equivalent for the infinite boson number. Indeed, the classical potential yields the same critical behavior as the energy functional since a minimum at $\tilde{\beta}=0$ obviously rises in the potential at η equal to

$$\eta_\infty^c=\frac{4}{5}, \tag{10}$$

which is just the $N\to\infty$ limit of Eq. (7). Note that the asymptotic independence of $\eta_N^c(\chi)$ on N is due to the $1/N$ scaling of the first term in Eq. (2). It should be pointed out here that the $\beta>0$ minimum of the potential (or energy functional) does not disappear at the critical η, but coexists with the $\beta=0$ minimum in a very narrow η region above the critical point (at first even preserving its role of the global minimum).

Before closing this section, we have to stress that the limit of infinite boson numbers has a key role for all effects connected with the IBM phase transition. In this limit, the condensate trial functions provide the exact representation of the IBM-1 eigenstates [16] and also the coherent states describe truly classical motions [18]—the model then has a purely geometrical interpretation and a classical counterpart. Therefore, the phase transition, as derived in both the above-mentioned approaches, is precisely defined only for $N\to\infty$. On the other hand, as will be demonstrated below, although the change of the eigenstate structure at $\eta=\eta_N^c(\chi)$ is not really discontinuous for finite boson numbers, it remains fast enough to keep the term ''critical'' (or quasicritical) sensible even in such cases.

III. SPECTROSCOPIC SIGNATURES OF THE PHASE TRANSITION

In this section, we will study spectroscopic properties of the Hamiltonian (2) along the SU(3)-U(5) transitional region. We therefore consider $\hat{H}_{(\eta,\chi)}$ with $\chi=-\sqrt{7}/2$ and look at the energies and wave functions of individual levels as they depend on η.

The standard treatment of the shape-phase transition based on the variational principle reflects explicitly only the ground-state properties. However, the structure of the ground state should influence also the excitation modes. Indeed, the change of form of the classical potential at the critical η signals a qualitative change of the quantum Hamiltonian (2) at the same place—the potential (8) is just an appropriate coordinate representation of the corresponding quantum operator—which means that the quasicritical behavior is expected also for excited states, at least those not too high in energy. This expectation is verified in Figs. 1 and 2.

Figure 1 shows the structure of the lowest-energy states with the angular momentum $J=0$, 2, and 4 (parity is always positive in the IBM-1). Exact (numerical) wave functions of these states in the SU(3)-U(5) transitional region were expanded in both the unperturbed SU(3) and U(5) bases. At $\eta=0$, the SU(3) expansion has just one component, while the U(5) expansion is trivial at $\eta=1$. In the $\eta\in(0,1)$ region, on the other hand, the real eigenstates are spread over all the U(5) and SU(3) eigenstates with the same angular momentum. The curves on the right-hand side of Fig. 1 (those increasing with η) represent the admixture (the squared modulus of amplitude) of the U(5) state 0_1^+, 2_1^+, or 4_1^+ in the actual state 0_1^+, 2_1^+, and 4_1^+, respectively. The left curves (decreasing) show the same for the SU(3) admixtures. This all is given for boson numbers $N=10$, 20, and 30.

Naturally, the SU(3) admixture shown in Fig. 1 drops from 1 to 0, as it must, and the U(5) admixture goes opposite. A more interesting feature is that while the SU(3) admixture decreases to zero gradually, in a wide region of η between 0 and ≈ 0.8, almost the whole $0\to1$ increase of the U(5) admixture takes place in a relatively narrow region

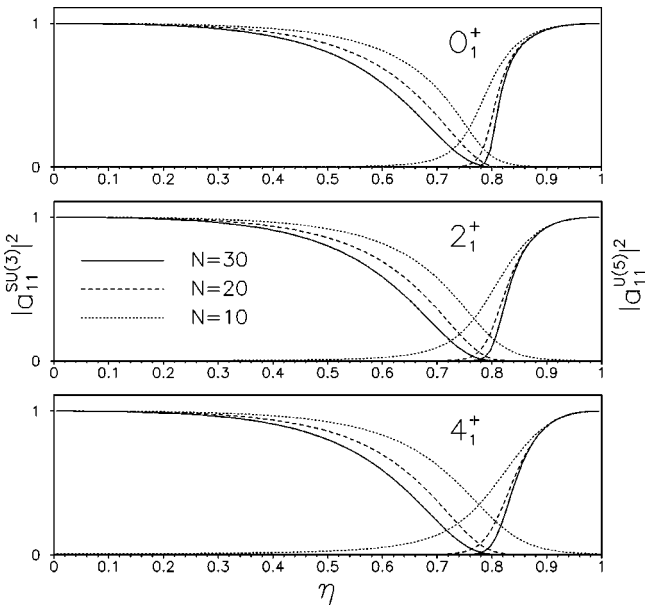

FIG. 1. Structural changes of the first 0^+, 2^+, and 4^+ states (upper, middle, and bottom panel, respectively) along the SU(3)-U(5) transition. Admixtures (squared amplitudes) of the unperturbed SU(3) and U(5) $J_k^\pi=0_1^+$, 2_1^+, and 4_1^+ state in the corresponding J_k^π transitional state are shown for various boson numbers. The onset of the U(5) structure has a critical behavior.

close to $\eta=0.8\equiv\eta_\infty^c$, i.e., around the critical point (7). The transition becomes apparently sharper as the excitation decreases and also for larger boson numbers. This all is compatible with the above explanations. The reason why the SU(3) admixture does not behave critically is that the potential minimum at $\beta>0$, existing below $\eta\approx0.8$, does not stay at a fixed position but moves gradually as η varies. Therefore, the overlap of an actual eigenstate for $\eta\in(0,0.8)$ with the corresponding $\eta=0$ eigenstate is imperfect even for infinite boson numbers.

Figure 2 shows the ratio $E(2_1^+)/E(4_1^+)$ of excitation energies (measured from the ground state 0_1^+) of the lowest 2^+ and 4^+ states. The ratio equal to 0.3 indicates the spectrum of an ideal rotor whereas the value of 0.5 is typical for a harmonic vibrator. Indeed, these values characterize the SU(3) and U(5) limits in Fig. 2—the vibrational character of

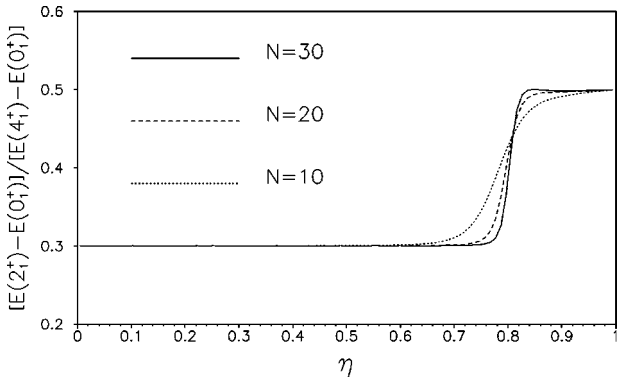

FIG. 2. A ratio of excitation energies of the first 2^+ and 4^+ levels along the SU(3)-U(5) transition. The flip between the rotational and vibrational limits is very sudden even for low boson numbers.

the low-energy spectrum is associated with a spherical drop while the rotational spectrum implies some deformation. As apparent from the figure, however, the switch between these two limiting regimes is very sudden even for boson numbers as low as $N=10$, which was shown [20,21] to have measurable consequences in real nuclei.

It is known that rapid structural changes of the $\hat{H}_\lambda$ eigenstates $\{|\Phi_\lambda^k\rangle\}$ are typically correlated with some specific variations of the eigenspectrum $\{E_\lambda^k\}$, namely with the so-called avoided level crossings, i.e., mutual approaching of two or more levels with the same symmetry quantum numbers. It can be easily shown that at the avoided-crossing places the mutual mixing of eigenstate is most efficient. Indeed, as the parameter value in Eq. (1) shifts from λ to $\lambda+\delta\lambda$, new eigenstates become mixtures of the old ones, the rate of mixing of the ith and jth state (both with the same symmetry quantum numbers) being expressed in the following way:

$$\lim_{\delta\lambda\to0}\frac{1}{\delta\lambda}\langle\Phi_\lambda^i|\Phi_{\lambda+\delta\lambda}^j\rangle\equiv\left\langle\Phi_\lambda^i\left|\frac{d}{d\lambda}\Phi_\lambda^j\right.\right\rangle=\frac{\langle\Phi_\lambda^i|\hat{H}_1-\hat{H}_0|\Phi_\lambda^j\rangle}{E_\lambda^j-E_\lambda^i}. \tag{11}$$

The energy difference in the denominator of the last expression clearly implies an acceleration of mixing if the two levels become close.

This general conclusion can be illustrated by considering the wave-function entropy in a simple two- or three-level system. The wave-function entropy of a state $|\psi\rangle$ with respect to a given reference basis $\mathcal{B}\equiv\{|i^{\mathcal{B}}\rangle\}_{i=1}^n$ is just the information entropy of the $|\psi\rangle$ distribution over the basis states:

$$W^{\mathcal{B}}(\psi)=-\sum_{i=1}^n|a_i^{\mathcal{B}}(\psi)|^2\ln|a_i^{\mathcal{B}}(\psi)|^2,\quad a_i^{\mathcal{B}}(\psi)=\langle i^{\mathcal{B}}|\psi\rangle. \tag{12}$$

It has been used by a number of authors (see, e.g., Refs. [23,24,15] and references therein) for measuring the above-mentioned effects of mixing. Indeed, if $|\psi\rangle$ coincides with one of the $\mathcal{B}$-states, its entropy (with respect to $\mathcal{B}$) is minimal, equal to 0, while if $|\psi\rangle$ is uniformly spread over all the n basis states, the entropy yields the maximal possible value, $\ln n$. Note that the relation of the information entropy to von Neumann basis-independent entropy was discussed in Ref. [25] along with some instructive examples.

We consider first, as the simplest example, a two-level mixing given by the following Hamiltonian:

$$H_\lambda^{(2)}=H_{\rm diag}^{(2)}+\lambda\dot{H}^{(2)}=\begin{pmatrix}-e+\dot{e}\lambda & \dot{v}\lambda\\ \dot{v}\lambda & e-\dot{e}\lambda\end{pmatrix}. \tag{13}$$

The wave-function entropy of both the Hamiltonian eigenstates in the basis $\mathcal{B}\equiv\{\binom{1}{0},\binom{0}{1}\}$ depends on the value of $x=(e-\dot{e}\lambda)/\dot{v}\lambda$, having a sharp maximum $[W^{\mathcal{B}}(1)=W^{\mathcal{B}}(2)=\ln2]$ at $x=0$. Therefore, the entropy increases with λ from 0 (for $\lambda=0$) to $\ln2$ (for $\lambda=e/\dot{e}$) and then decreases again to a limiting value ($\lambda\to\infty$) determined by

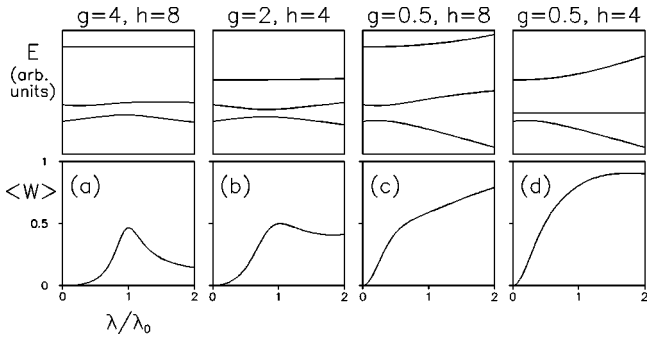

FIG. 3. The spectrum and average wave-function entropy of the eigenstates of the three-state Hamiltonian (14) as a function of λ. The spectra, shown in the upper panels for various choices of constants (see the text), are accompanied in the lower panels by the corresponding average entropies with respect to the $\lambda=0$ eigenbasis. The avoided crossings of the lower two levels apparently accelerate the mixing process, regardless of whether it results in just an exchange (more or less) of unperturbed wave functions for large λ (left) or in their complete spread out (right).

the ratio $\dot{e}/\dot{v}$. The maximum rate of mixing is thus connected with the avoided crossing of both the levels.

A bit more complex behavior is characteristic for a three-level system,

$$H_{\lambda}^{(3)}=H_{\mathrm{diag}}^{(3)}+\lambda\dot{H}^{(3)}=\begin{pmatrix} e_0 & \dot{w}\lambda & \dot{w}\lambda \\ \dot{w}\lambda & -e+\dot{e}\lambda & \dot{v}\lambda \\ \dot{w}\lambda & \dot{v}\lambda & e-\dot{e}\lambda \end{pmatrix}, \tag{14}$$

describing again the two-state mixing, but influenced by a third state. Figure 3 shows the energy spectrum and the corresponding average wave-function entropy (again in the $\lambda=0$ eigenbasis, the averaging involves all three states) as a function of $\lambda/\lambda_0=\lambda\dot{e}/e$ for different values of $\dot{w}/\dot{v}\equiv f$ and $\dot{e}/\dot{v}\equiv g$ (we consider $e_0/e\equiv h=1$). Common to all the typical patterns shown in panels (a)–(d) is the fact that the entropy grows most rapidly when the lower two states become closest. Note that although the Hamiltonian (14) contains nominally five constants, the only ones relevant for the present analysis are the above dimensionless ratios *f*, *g*, and *h*.

These principles can be applied also to the interacting boson model. Figure 4 shows a correlation between the level dynamics and wave-function entropies for the 0^+ eigenstates of the Hamiltonian (2) in the case of $N=30$. In the upper part, the energy spectrum of all 0^+ states is displayed as it varies with η along the SU(3)-U(5) transition (the ground-state energy is constantly set to 0 here), while the corresponding wave-function entropies in the U(5) and SU(3) bases are shown—for two selected states—in the lower part (unlike Fig. 3, the entropies characterize only the given single state here). A manifold avoided crossing of levels, situated just to the phase-transitional region $\eta\approx 0.8$, is apparently responsible for the basic variations of the wave-function entropies. The correspondence between the upper and lower parts of Fig. 4 persists even under the scrutiny, when the oscillations in the 0_4^+-state entropy are found to

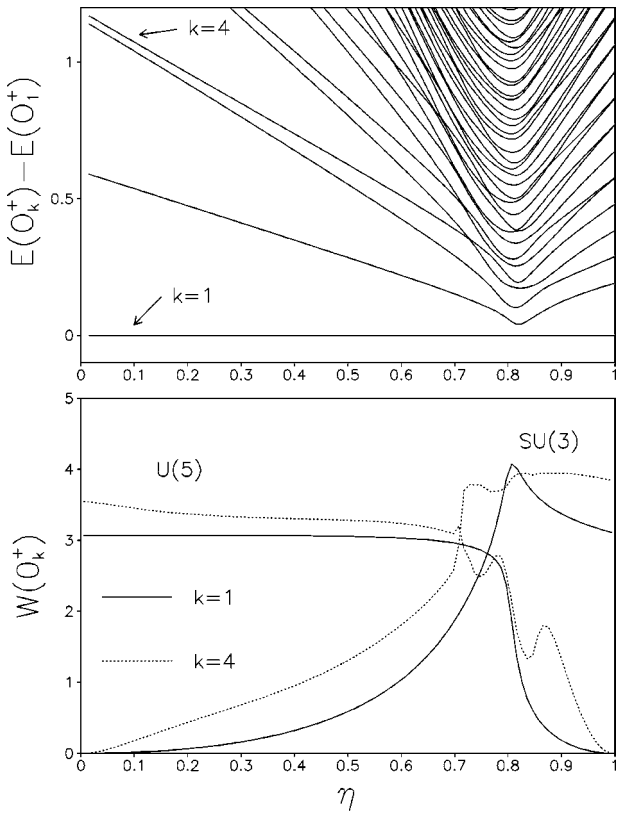

FIG. 4. The spectrum of 0^+ states (with the ground-state energy set to 0) along the SU(3)-U(5) transition (upper part) and the corresponding wave-function entropy of the first and fourth state in the U(5) and SU(3) bases (lower part) for $N=30$. Major as well as minor variations of the wave-function entropy are correlated with the avoided level crossings.

exactly coincide with the single avoided level crossings of the 0_4^+ level with its neighbors. Note that the structural oscillations of individual eigenstates, like those shown here for the 0_4^+ state, occur quite generally in parameter-dependent quantum systems and can have drastic consequences for the behavior of transition probabilities [22].

We just saw that the ''macroscopic'' flip of the eigenstate structure at $\eta\approx 0.8$ is correlated with (one even tends to say ''caused by'') a simultaneous avoided crossing of many levels at the same parameter value. This conclusion, verified also in other quantum systems possessing critical behaviors [4,5,8], leads to a natural question of what makes the levels behave in such a peculiar way. The true origin of this phenomenon is clearly the qualitative change of the Hamiltonian at the critical point, namely the rise of the $\beta=0$ potential minimum. It is known that the connection between the Hamiltonian and level dynamics goes via the notion of so-called exceptional points (also branch or crossing points) [4,5,26–28]. Exceptional points of the Hamiltonian $\hat{H}_{\lambda}$ are defined if the range of λ is extended to the complex plane—they represent those complex parameter values where two (or more) different levels become degenerated. Note that the well-known rule that energy levels do not really cross, in generic cases, if just one Hamiltonian parameter is varied [29] is right for real λ only. Exceptional points have a similar relation to the avoided level crossings as the *S*-matrix poles to cross-section resonances: if an exceptional point is

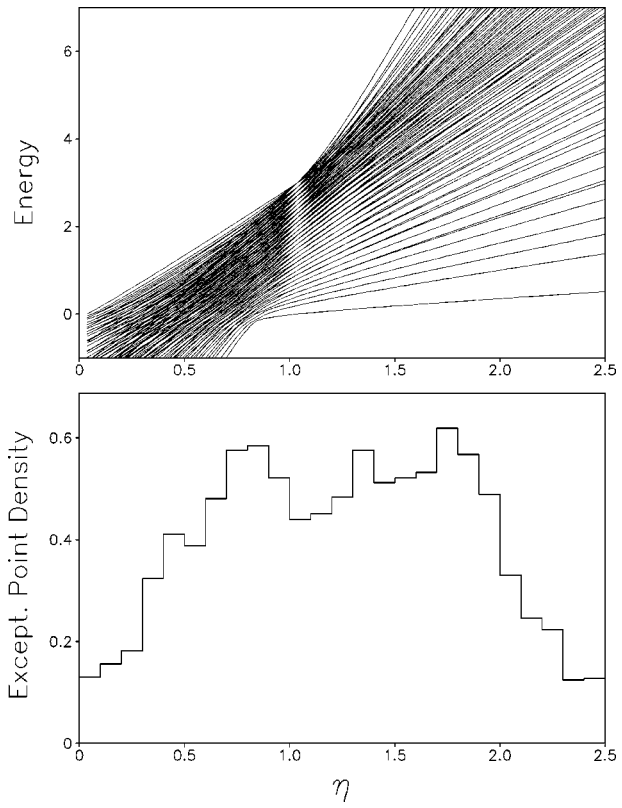

FIG. 5. The ''dynamics'' of 0^+ states ($N=30$) induced by the change of parameter $\eta\in[0,2.5]$ (upper panel) and the accompanying (approximative) distribution of the exceptional-point real parts (lower panel). The peaks in the exceptional-point distribution correspond to multiple avoided crossings of levels.

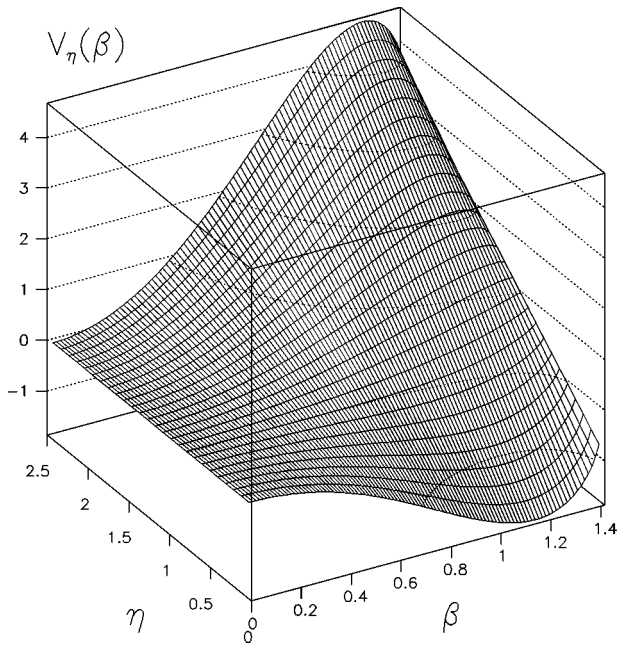

FIG. 6. The potential (8) as a function of $\tilde{\beta}$ (with $\tilde{\gamma}=0$) for $\eta\in[0,2.5]$ and $\chi=-\sqrt{7}/2$. The potential minimum moves from $\tilde{\beta}\approx1.2$ to $\tilde{\beta}=0$ at $\eta=0.8$ and the $\tilde{\beta}\approx1.2$ maximum rises at $\eta=1$. These features are behind the phenomena shown in Fig. 5.

close to the real-λ axis, the avoided crossing of the corresponding levels is located at that place. Thus, the phase-transitional behavior of a quantum system is encountered at $\lambda=\lambda^c$ if some (many) of the exceptional points are aligned in parallel to the imaginary axis with $\mathrm{Re}\,\lambda=\lambda^c$ [4,5].

We calculated the distribution of exceptional points of the Hamiltonian (2) along the real parameter axis, i.e., the density of the exceptional-η real parts. The method used, taken from Ref. [28], is only approximative—based on the asymptotic behavior of the spectrum for large η—but accurate enough for our purposes. The result for 0^+ states with $N=30$ is shown in Fig. 5 (lower part) together with the corresponding energy spectrum (upper part) in the parameter range $\eta\in[0,2.5]$ (the reason for considering also $\eta>1$ will be clarified later). First of all, the level energies are now plotted without subtracting the ground-state energy, which discloses some new features disregarded in the presentation of Fig. 4. In particular, at the critical point the bunch of level ''trajectories'' is squeezed in such a way that the slope changes more for low-energy levels than for the high-energy ones (the highest-energy states remain completely unaffected). This can be easily understood in terms of the potential (8) shown for the corresponding η region in Fig. 6 with $\gamma=0$. The potential change at the critical η influences only the states whose average kinetic energy does not exceed much the depth of the $\beta=0$ minimum; for the ground state the slopes below and above $\eta\approx0.8$ correspond approximately to the elevation rate of the global potential minimum in the respective regions [be reminded that for $N\to\infty$ the condensate states (5) become exact eigenstates and Eq. (6) thus yields exact energies]. Associated with the spectrum compression at the critical point is the well pronounced peak in the exceptional-point distribution in the lower panel of Fig. 5. We therefore confirm that the switch of the potential form influences the avoided-crossing pattern through the partial alignment of the Hamiltonian exceptional points.

However, the $\eta\approx0.8$ peak in the exceptional-point density in Fig. 5 is not the only one. An increase is observed also in the region $\eta\in(1,2)$, where, as apparent in the upper panel of Fig. 5, another change of the slope of levels occur, similar to the one at $\eta\approx0.8$ but affecting in contrary only the high-energy states. We have to first emphasize that although the Hamiltonian (2) was originally considered only in the range $\eta\in[0,1]$, the present values of $\eta>1$ (in fact, all values $-\infty<\eta<+\infty$) still yield perfectly acceptable IBM-1 Hamiltonians. They are also transitional between the U(5) and SU(3) symmetries (see the expansions of $\hat{H}_{(\eta,\chi)}$ into Casimir invariants given in Ref. [15]), just like the $\eta\in[0,1]$ ones (which was the reason for not considering them in the original parametrization), but exhibit effects inequivalent to those present in the restricted interval. Comparing Figs. 5 and 6, one sees that the cumulation of exceptional points in the region $\eta>1$ is connected with another qualitative change of the potential, the rise of the $\tilde{\beta}\approx1.2$ maximum. At the corresponding parameter value, i.e., at $\eta=1$ [see Eq. (8)], the global potential maximum moves from $\tilde{\beta}=\sqrt{2}$ to the new position and the rate of its increase with η changes. For sufficiently large boson numbers, the same behavior must characterize also the highest excitation energy, since Eq. (6) describes the true eigenspectrum for $N\to\infty$. The level dynamics shown in Fig. 5 apparently confirms these considerations.

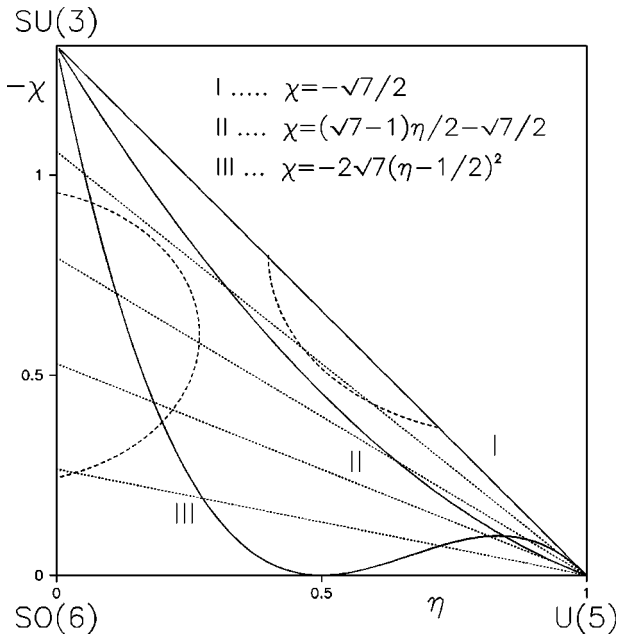

FIG. 7. The Casten triangle for the (η,χ)-parameter sheet of the Hamiltonian (2) and the paths I–III between the U(5) and SU(3) dynamical symmetries, as considered in Sec. IV. The dashed semicircles schematically indicate the most chaotic regions.

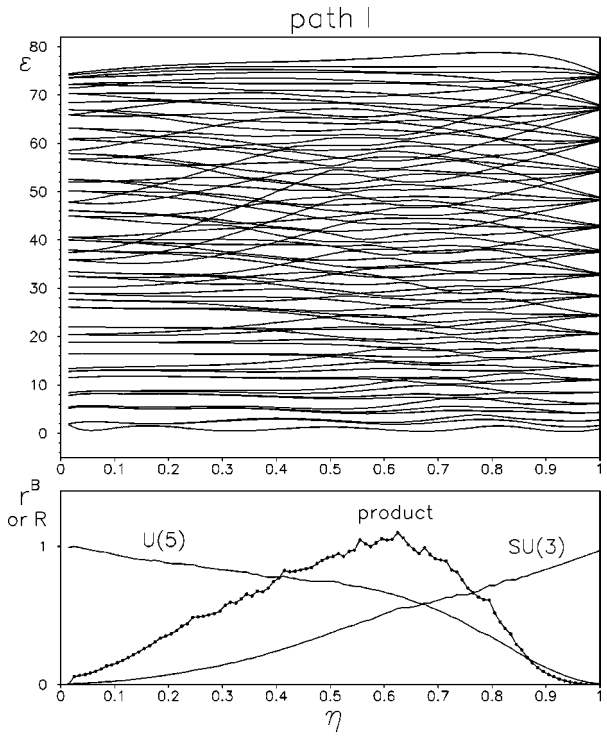

FIG. 8. The ''dynamics'' of the unfolded spectrum of 2^+ states ($N=20$) for the U(5)-SU(3) path I (upper panel) and the corresponding entropic measures of chaos (lower panel). The U(5) and SU(3) entropy ratios quantify the average overlap of the actual 2^+ states with bases in the respective symmetry limits, while the entropy-ratio product measures the overall degree of chaos.

IV. DYNAMICAL CONSEQUENCES

The importance of avoided level crossings in nonstationary quantum problems is generally known. In particular, the mechanism of so-called Landau-Zener transitions [30] is often mentioned in the literature. Suppose that the parameter λ in Eq. (1) is made time dependent—consider the simplest dependence $\lambda(t)=\dot{\lambda}t$ at the moment—and that the system is initially prepared in one of the $\hat{H}_0$ eigenstates, $|\Phi_0^i\rangle$. Because jumps between various eigenstates occur most likely at the avoided-crossing places, the probability of finding the ith eigenstate, $|\Phi_{\lambda(t)}^i\rangle$, at a time $t>0$ depends very much on the way in which the levels between the ith and jth ''collide'' with each other within the corresponding parameter interval. The transition probability is also sensitive to the rate of the parameter change: in the limiting adiabatic (infinitely slow) regime the system exactly follows the state $|\Phi_{\lambda(t)}^i\rangle$ with no chance to jump, which is certainly very different from a typical behavior if the change is fast (close to the diabatic limit). It is obvious that the most pronounced differences between fast and slow dynamics must be connected with the spectral regions containing a large number of avoided level crossings. Practical implications of such investigations are numerous; remember, for example, elastoplastic and memory effects in nuclear large-amplitude motions [31,32] or other peculiar phenomena studied so far mostly in some schematic models—see, e.g., Refs. [33,34].

In this section we focus on a few nonstationary problems related to the IBM Hamiltonian (2). The reason for such a study is the expectation that the multiple avoided crossing of levels at the phase-separating curve (7) may have interesting consequences for the dynamics induced by some driven variations of the model parameters. It should be stressed from the very beginning that we do not pretend to make here a complete account of all such dynamical phase-transitional effects; rather we try to give some hints that will hopefully inspire a more detailed analysis.

In contrast to Sec. III, we allow for variations of both the $\hat{H}_{(\eta,\chi)}$ parameters. It is expressed by a functional dependence of χ upon η: as η varies between 0 and 1, χ changes accordingly. In particular, we consider three paths from the U(5) to SU(3) limit (i.e., η goes down from 1 to 0), given by the following formulas:

$$\chi(\eta)=\begin{cases} -\dfrac{\sqrt{7}}{2} & \text{for path I} \\ \dfrac{\sqrt{7}-1}{2}\,\eta-\dfrac{\sqrt{7}}{2} & \text{for path II} \\ -2\sqrt{7}\left(\eta-\dfrac{1}{2}\right)^2 & \text{for path III.} \end{cases} \tag{15}$$

Whereas path I is the one from Sec. III, the two additional paths go through the interior of the Casten triangle—see Fig. 7. The choice of the paths I–III is motivated by the fact that they cross regions of the parameter sheet characterized by different quantum and classical degrees of chaos, as described in Ref. [13]: whereas I and III pass through two different chaotic regions at medium and small η, respectively, the path II follows the semiregular ''valley'' in between both the chaotic regions (see the schematic view in Fig. 7). For each path, the Hamiltonian $\hat{H}_{(\eta,\chi)}$ can be written

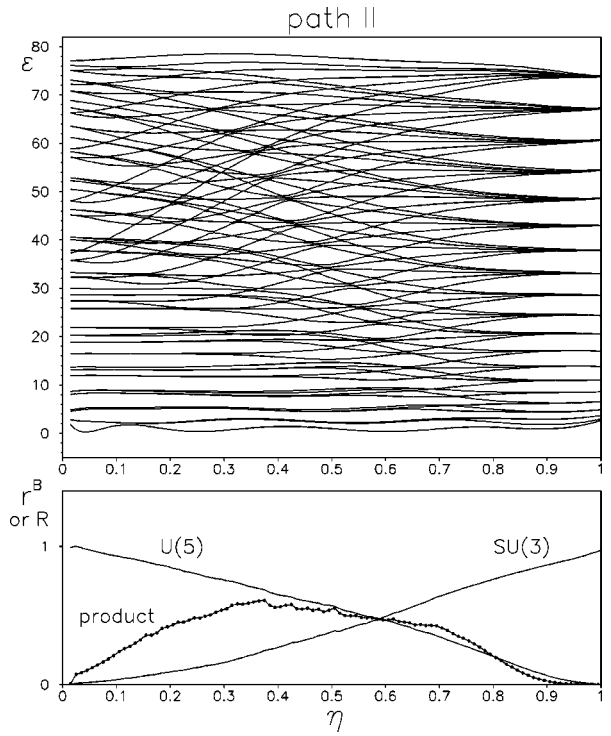

FIG. 9. The same as in Fig. 8 but for the path II. The entropy-ratio product, lower compared to Fig. 8, indicates a suppression of chaos, which seems to be connected with the particular ''moving'' structure of level bunchings.

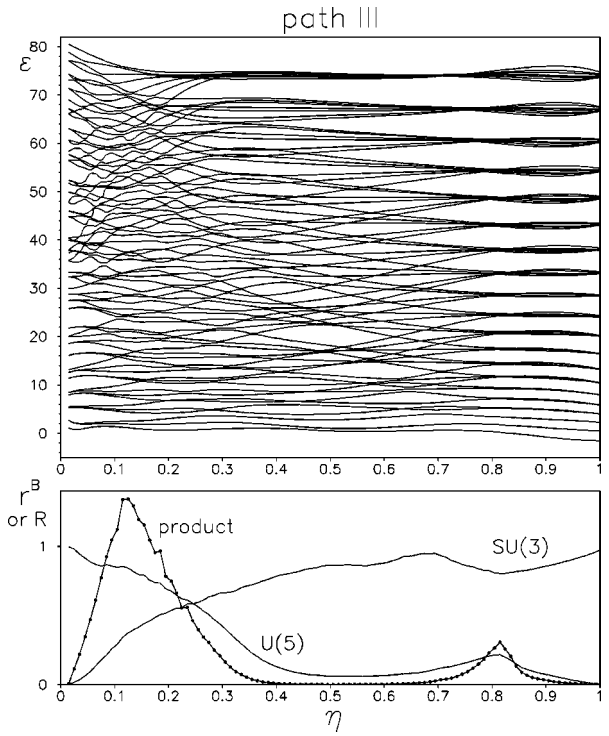

FIG. 10. The same as in Fig. 8 but for the path III. Regular as well as chaotic regions are crossed, as indicated by the entropy-ratio product. In contrast to Fig. 8, the $\eta<0.3$ chaotic region shows a turbulent ''flow'' of levels.

as $\hat{H}_\eta$ if the respective dependence $\chi(\eta)$ is substituted, and it becomes a particular function of time if η is driven according to a function $\eta(t)$.

To illustrate the above-mentioned features related to chaos, we present in Figs. 8–10 unfolded spectra of the 2^+ states for $N=20$ together with the corresponding average wave-function entropies for all the paths I–III. Be reminded that the spectral unfolding is a special transformation of level energies, which ensures that the resulting spectra are free of ''secular variations'' of the level density and are thus prepared for studying fluctuations and correlations, as usual in the theory of quantum chaos. The unfolding procedure described in Ref. [35] was employed here, which is based on fitting the staircase function $N(J^\pi,E,\eta)$, the number of J^π levels below energy E, by a two-dimensional (E,η) polynomial and evaluating the smooth part of the level density from the fitted function. As a result, the transformation $E_i(\eta) \rightarrow \varepsilon_i(\eta)$ is obtained, where the average spacing $\langle \varepsilon_{i+1}-\varepsilon_i \rangle$ is constant (≈ 1) throughout the whole transformed spectrum—see Figs. 8–10.

We do not show here the quantal measures of chaos derived from the unfolded spectra in Figs. 8–10, as this analysis was done for the whole Casten triangle in Ref. [13]. One can directly see, however, that the unfolded-level statistics interpolates the whole range between the chaotic case (with a strong level repulsion) and the regular case (with a considerable bunching of levels). It is interesting that neither the U(5) nor SU(3) limits yield the level statistics generic for integrable systems, as was observed in Refs. [13,36]. Also noticed should be the level dynamics with a peculiar pattern of bunchings found for path II—see Fig. 9. The sequence of bunchings, descending in energy as η goes from ≈ 0.3 to 0.7, clearly pushes the level statistics towards the Poissonian case and thus contributes to the result that the corresponding region of the Casten triangle is quasiregular [13]. Whether this quasiregularity is caused by some hidden partial symmetry is still unclear, but the pattern shown in Fig. 9 might be a hint.

The U(5) and SU(3) entropy ratios and the entropy-ratio product, shown in the lower panels of Figs. 8–10, are derived from the average wave-function entropies of the 2^+ eigenstates in bases corresponding to the various dynamical symmetries. In particular, the entropy ratio $r^{\mathcal{B}}$ derived from the wave-function entropy $W^{\mathcal{B}}$ (average over all 2^+ states in our case) is defined [14,15] as $r^{\mathcal{B}}=\mathcal{N}(\exp W^{\mathcal{B}}-1)$, where the scaling coefficient $\mathcal{N}$ ensures that $r^{\mathcal{B}}\approx 1$ for any ensemble of eigenstates that exhibit a random overlap with the reference basis $\mathcal{B}$ (the expression for $\mathcal{N}$ contains in the denominator the average entropy of eigenstates of a random-matrix ensemble, see Ref. [15], which justifies the term ''entropy ratio''). Figures 8–10 show the entropy ratios with respect to the U(5) and SU(3) bases as a function of η for the three paths between the SU(3) and U(5) limits. It is evident that the phase-transitional behavior is washed out in the average containing all the 2^+ eigenstates (see also [15]).

The entropy-ratio product R, also shown in Figs. 8–10, is defined [14,15] as a product of the entropy ratios over the bases $\mathcal{B}$ associated with all dynamical symmetries of the model. Expressing something like a content of dynamical symmetries in a particular Hamiltonian $\hat{H}_{(\eta,\chi)}$, the entropy-ratio product R was found [14,15] to be perfectly correlated with quantal measures of chaos corresponding to the given $\hat{H}_{(\eta,\chi)}$. Indeed, the behavior of R shown in the lower panels of Figs. 8–10 is in agreement with the localization of chaotic

and regular regions in the Casten triangle, as schematically represented in Fig. 7. In particular, path II (Fig. 9) crossing the above-mentioned quasiregular region yields much lower R than path I (Fig. 8), which goes directly through the chaotic region at the SU(3)-U(5) leg. Also Fig. 10 exhibits a large maximum of R when path III ranges through the chaotic region at the SO(6)-SU(3) leg, while R is in contrast negligible when the path is close to the integrable SO(6)-U(5) region. The small maximum of R at $\eta \approx 0.8$ in Fig. 10 is due to the deviation of path III from the chaotic SU(3)-U(5) region towards the regular SO(6)-U(5) region; it is also clearly correlated with the multiple avoided crossings of levels in the upper panel of Fig. 10.

It is clear that the unfolded spectra in Figs. 8–10 do not exhibit the characteristic phase-transitional behavior shown in Figs. 4 and 5; it was removed by the unfolding. In the following we will show, however, that the waving curves of unfolded-level energies still carry—besides their apparent aesthetic appeal—physical information important for the dynamics induced by the driven variations $(\eta,\chi)(t)$ along paths I–III. In particular, the ''laminar'' and ''turbulent'' character of the ''flow'' of unfolded levels is contrasted. One can notice that whereas the chaotic region crossed by the path I yields a laminar flow, see Fig. 8, the chaotic region crossed by path III yields in contrast a turbulent flow in the upper part of the spectrum, see Fig. 10. The laminar flow implies a small number of avoided level crossings and leads therefore to a more or less steady rate of the eigenstate mixing. The turbulent flow, on the other hand, develops through many avoided crossings and thus induces dramatic rearrangements of eigenfunctions. This means that differences between slow and fast parameter variations and other memory effects, as mentioned above, must be expected to play the most important role if the turbulent flow of levels is encountered.

To confirm these qualitative considerations, we have calculated the average energy and its η derivative, a ''force,'' in case of adiabatic and diabatic transitions between the U(5) and SU(3) limits along the three paths in Eq. (15). In particular, we assumed the system, characterized by an inverse temperature $\beta = 1/T$, being at first in the U(5) limit, i.e., at $\eta = 1$. Within the adiabatic change, the thermal equilibrium is established at each new parameter value, so that the canonical occupation probabilities always characterize the population of the actual energy eigenstates. The energy average at any value of η is then given by the following formula:

$$\langle E_\eta^{\mathrm{adiab}} \rangle_\beta \equiv \frac{\mathrm{Tr}(\hat{H}_\eta e^{-\beta \hat{H}_\eta})}{\mathrm{Tr}\, e^{-\beta \hat{H}_\eta}} = \frac{\sum_i E_\eta^i e^{-\beta E_\eta^i}}{\sum_i e^{-\beta E_\eta^i}}. \tag{16}$$

On the other hand, the diabatic change is so fast that the system has no time to move from its initial state and thus deviates from the actual thermal equilibrium. We have

$$\langle E_\eta^{\mathrm{diab}} \rangle_\beta \equiv \frac{\mathrm{Tr}(\hat{H}_\eta e^{-\beta \hat{H}_1})}{\mathrm{Tr}\, e^{-\beta \hat{H}_1}} = \frac{\sum_i E_\eta^i \sum_j |\langle \Phi_\eta^i | \Phi_1^j \rangle|^2 e^{-\beta E_\eta^j}}{\sum_i e^{-\beta E_1^i}}. \tag{17}$$

The use of the canonical density operator $\hat{\rho} \propto \exp(-\beta \hat{H})$, either adiabatic or diabatic, can in our case be advocated by its simplicity: the variable population of levels that we need to incorporate into our calculations is controlled here just by a single parameter, β. However, for our purposes, the standard thermal population is disadvantageous as it gives lesser weights to higher excited states compared to those near to the ground state. Indeed, in view of the discussion regarding spectra in Figs. 8 –10 we need to consider also the inverse population of states, i.e., negative temperatures. We therefore allow for any value $\beta \in (-\infty, +\infty)$ and introduce a new variable,

$$x(\beta) = \begin{cases} e^{-\beta} & \text{for } \beta \geqslant 0 \\ 2 - e^{\beta} & \text{for } \beta < 0, \end{cases} \tag{18}$$

which changes between $x(\beta) = 0$ for $T = +0$ (i.e., only the ground state populated) and $x(\beta) = 2$ for $T = -0$ (only the highest state populated), the intermediate value $x(\beta) = 1$ being attributed to $T = \pm\infty$ (a uniform population of all states). To avoid possible confusion, it should be stressed that here the negative temperatures are just a formal tool to describe dynamical features related to high-energy parts of spectra in Figs. 8–10; any deeper physical justification of their use would be misleading at the moment.

Now we are in a position to explain the main physical result of this section, presented in Fig. 11. We calculated the average energy $\langle E_\eta \rangle_\beta$ and the ''force'' $d\langle E_\eta \rangle_\beta / d\eta$ as a function of $1 - \eta \in [0,1]$ for the 2^+ states at $N = 20$ shown in Figs. 8–10 (note that the term ''force'' for the η derivative of energy results from an obvious generalization of the classical relation $dE = F dx$). The calculation was done for (a) both the adiabatic and diabatic limits, (b) all three paths I–III, and for (c) the whole interval $x(\beta) \in [0,2]$. In Fig. 11, the force (the leftmost and middle columns) is presented for the whole interval (c), while the average energy (the rightmost column) is shown only for the limiting values of $x(\beta) = 0$ and 1. The aim pursued was to find differences between the adiabatic and diabatic dynamics, i.e., indications for dynamical memory effects.

The main message of Fig. 11 can be put as follows: the most pronounced memory effects in the U(5)→SU(3) transition—at least as far as the force is concerned—are connected with the spectral regions with a large density of avoided level crossings. It is, with the low-energy region near the critical point $\eta \approx 0.8$ (like in Fig. 5) and for the path III also with the ''turbulent'' high-energy region at $\eta < 0.3$ (see Fig. 10). The low-energy crossings near the critical point (cf. Fig. 5) induce the adiabatic-diabatic difference of the force at low positive temperatures $[x(\beta) \approx 0]$, while the high-energy crossings in the small-η region of path III (Fig. 10) induce the difference at negative temperatures close to zero $[x(\beta) \approx 2]$—see the leftmost and middle columns of Fig. 11.

The steplike adiabatic evolution of the force for $x(\beta) \approx 0$ (see the leftmost column of Fig. 11) is connected with a change of the slope of low-lying 2^+ levels near the critical η, similar to that shown for 0^+ states in Fig. 5. This is shown in the rightmost column of Fig. 11 for the lowest 2^+ state by the lower full curves [adiabatic energy average with

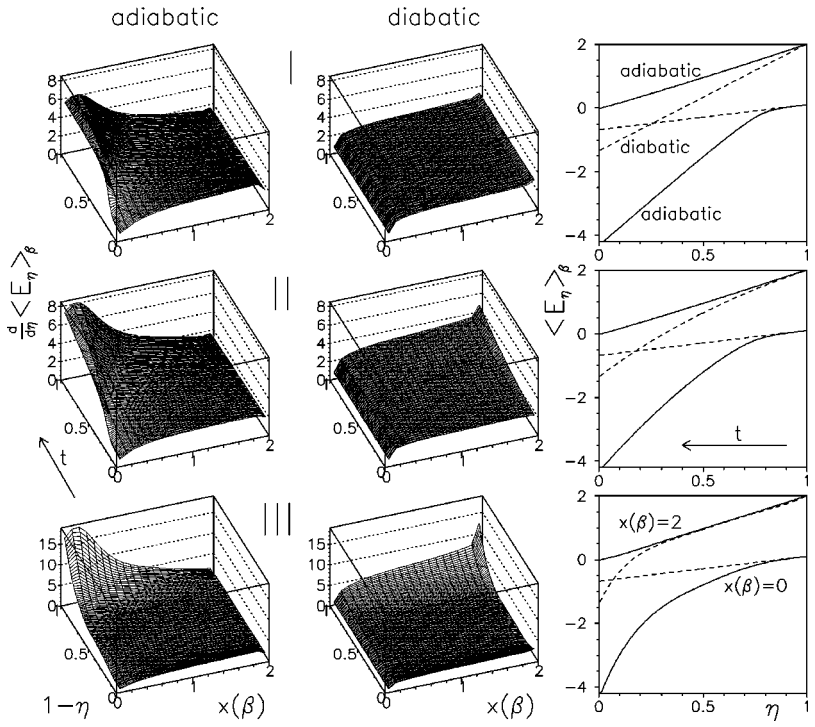

FIG. 11. The adiabatic and diabatic change of the thermal average energy of 2^+ states for $N=20$ (column on the right) and the corresponding ''force'' (left and middle columns) along the U(5)→SU(3) ($\eta=1\rightarrow0$) paths I–III (rows from top to bottom). Both positive and negative temperatures were considered in Eqs. (16) and (17), the results being presented as a function of $x(\beta)$ from Eq. (18). The differences between adiabatic and diabatic behavior of the force (memory effects) are well pronounced in the $\eta\times x(\beta)$ regions with a large number of avoided level crossings located in the corresponding spectral region. Besides the multiple avoided level crossing at the critical η, also the crossings in the ''turbulent'' area in Fig. 10 play an important role.

$x(\beta)=0$]. The diabatic energy average, shown for $x(\beta)=0$ by the lower dashed curves, exhibits in contrary no change of slope, which leads to a force constant over the whole transitional region (see the middle column of Fig. 11). Let us stress again that this difference between the adiabatic and diabatic behaviors is connected with the structural rearrangements of eigenstates induced by the phase transition. Because the avoided crossing at the critical point involves many levels, the diabatic evolutions most likely change the $|\Phi^0_\eta\rangle$ state ($\eta>0.8$) into a quantum mixture of a large number of $|\Phi^i_\eta\rangle$ eigenstates at $\eta<0.8$. This is why the diabatic energy average for $x(\beta)=0$ goes steadily off the adiabatic average below $\eta\approx0.8$ (note that for a constant χ the diabatic force must be totally independent of η—see box I in the middle column of Fig. 11).

The adiabatic energy average with $x(\beta)=2$ (upper full curves in the rightmost column of Fig. 11), which represents the energy of the highest 2^+ state, exhibits no change of slope and therefore implies a constant adiabatic force near $x(\beta)\approx2$. On the other hand, the diabatic energy average with $x(\beta)=2$ (upper dashed curves in the rightmost column) varies in a different way, the most important deviation from the adiabatic case being observed in the $\eta<0.3$ region for path III. This implies the increase of the path-III diabatic force near $x(\beta)\approx2$. The $x(\beta)=2$ diabatic energy average for path III clearly corresponds to the trajectory that we see in the ''turbulent'' part of the spectrum in Fig. 10 with half-open eyes. The present memory effect is thus again connected with the pattern of avoided level crossings, or more precisely, with the accompanying structural changes of wave functions.

As was pointed out above, the present analysis is mainly intended as an initialization of some more detailed works. In particular, we believe that the nonstationary problems connected with phase-transitional quantum systems might have some impact in the theory of quantum dissipation and related areas—see, e.g., Refs. [37–39]. As a simple example, consider a nucleus colliding with a projectile, the situation being characterized by a few ''macroscopic'' coordinates including shape parameters of the target nucleus. Now suppose a frictional mechanism, which transfers the initial kinetic energy of the system from the macroscopic motion into some nuclear internal degrees of freedom. It is clear that the internal dynamics depends on the nuclear shape parameters, which are, in the same time, among the macroscopic coordinates—these parameters thus mediate the coupling of both the internal and macroscopic degrees of freedom. We can assume the Hamiltonian (2) as describing the internal dynamics, the parameters η and χ being the above shape coordinates (in some generalized sense). Therefore, η and χ are not any more static or independently driven, as we considered them above; they become truly dynamical variables. We know that the internal dynamics undergoes a qualitative change at the critical (η,χ) border. How does this influence the evolution of the system, for instance, the energy transfer from macroscopic to internal degrees of freedom? In our opinion, the answers to these kinds of questions carry physically interesting information and may also turn out to be important in some realistic situations.

V. CONCLUSIONS

We studied quantum phase-transitional behavior in the interacting boson model 1. In literature, the shape-phase transition in this model is presented as a sharp qualitative change of the ground-state wave function for $N\rightarrow\infty$ or as a corresponding abrupt change of the classical potential. We showed, however, that spectroscopic signatures of the phase transition, still sharp enough even for boson numbers as low as $N=10$, are characteristic also for a large number of excited states (see Figs. 1, 2, 4). This phenomenon was related to the multiple avoided crossing of levels near the critical

parameter value, which is mediated by a partial alignment of the Hamiltonian exceptional points (Fig. 5). We then demonstrated, on the simplest example of driven adiabatic and diabatic parameter variations, that the phase-transitional behavior has a significant impact on memory effects in nonstationary quantum problems (Fig. 11).

Working in the above basic direction, several side results were obtained: (a) We derived a finite-N energy functional corresponding to the Hamiltonian (2), see Eq. (6), and the exact phase separatrix (7) in the parameter plane. (b) We showed that besides the $\eta=0.8$ phase transition, another qualitative change of the classical potential takes place at $\eta=1$ (Fig. 6). It causes a multiple avoided crossing of high-energy levels (see Fig. 5) and constitutes a new class of IBM-1 phase-transitional effects. (c) We calculated unfolded parameter-dependent energy spectra for three paths crossing parameter regions with different degrees of chaos (Figs. 8–10). It turned out that the fully chaotic regions can yield both the laminar and turbulent flow of levels, resulting in different dynamical memory effects (Fig. 11). Moreover, we disclosed a particular sequence of level bunchings (see Fig. 9) that can be significant for the quasiregular behavior observed [13] in the parameter region along path II.

To conclude, we point out that the study of phase transitions within the interacting boson model not only may open some new theoretical viewpoints, but it is also very relevant for the concrete physics of atomic nuclei. Spectroscopic signatures of a critical shape-phase transition were identified [20,21] in spectra of even-even nuclei, for which the IBM-1 provides an adequate description. The features studied here may thus turn out to have observable nuclear consequences. We believe that even the dynamical studies using the IBM, such as that involved in Sec. IV, can be found useful for the modeling of the energy transfer into internal collective degrees of freedom in heavy-ion collisions.

ACKNOWLEDGMENTS

This work was supported by the Grant Agency of the Charles University (Grant No. 38/97) and by the Swiss National Science Foundation. P.C. acknowledges an additional subsidy from the University of Fribourg.

[1] D. J. Rowe, Prog. Part. Nucl. Phys. **37**, 265 (1996).
[2] D. J. Thouless, Nucl. Phys. **22**, 78 (1961).
[3] E. D. Davis and W. D. Heiss, J. Phys. G **12**, 805 (1986).
[4] W. D. Heiss, Z. Phys. A **329**, 133 (1988); W. D. Heiss and A. A. Kotzé, *ibid.* **331**, 223 (1988).
[5] W. D. Heiss and A. L. Sannino, Phys. Rev. A **43**, 4159 (1991); W. D. Heiss, Phys. Rep. **242**, 443 (1994).
[6] D. H. Feng, R. Gilmore, and S. R. Deans, Phys. Rev. C **23**, 1254 (1981).
[7] A. E. Dieperink, O. Scholten, and F. Iachello, Phys. Rev. Lett. **44**, 1747 (1980).
[8] D. J. Rowe, C. Bahri, and W. Wijesundera, Phys. Rev. Lett. **80**, 4394 (1998).
[9] F. Iachello and A. Arima, *The Interacting Boson Model* (Cambridge University Press, Cambridge, England, 1987).
[10] A. Frank and P. Van Isacker, *Algebraic Methods in Molecular and Nuclear Structure Physics* (Wiley, New York, 1994).
[11] J. Dobeš, Phys. Rev. C **42**, 2023 (1990).
[12] P. Van Isacker, A. Frank, and J. Dukelsky, Phys. Rev. C **31**, 671 (1985).
[13] N. Whelan and Y. Alhassid, Nucl. Phys. A **556**, 42 (1993).
[14] P. Cejnar and J. Jolie, Phys. Lett. B **420**, 241 (1998).
[15] P. Cejnar and J. Jolie, Phys. Rev. E **58**, 387 (1998).
[16] J. N. Ginocchio and M. W. Kirson, Nucl. Phys. A **350**, 31 (1980).
[17] R. L. Hatch and S. Levit, Phys. Rev. C **25**, 614 (1982).
[18] Y. Alhassid and N. Whelan, Phys. Rev. C **43**, 2637 (1991).
[19] A. Klein and M. Vallieres, Phys. Rev. Lett. **46**, 586 (1981).
[20] R. F. Casten, N. V. Zamfir, and D. S. Brenner, Phys. Rev. Lett. **71**, 227 (1993).
[21] R. F. Casten, D. Kusnezov, and N. V. Zamfir, Phys. Rev. Lett. **82**, 5000 (1999).
[22] J. Jolie, P. Cejnar, and J. Dobeš, Phys. Rev. C **60**, 061303(R) (1999).
[23] F. M. Izrailev, Phys. Rep. **196**, 299 (1990).
[24] V. Zelevinsky, B. A. Brown, N. Frazier, and M. Horoi, Phys. Rep. **276**, 85 (1996).
[25] V. V. Sokolov, B. A. Brown, and V. Zelevinsky, Phys. Rev. E **58**, 56 (1998).
[26] M. R. Zirnbauer, J. J. M. Verbaarschot, and H. A. Weidenmüller, Nucl. Phys. A **441**, 161 (1983).
[27] P. E. Shanley, Ann. Phys. (N.Y.) **186**, 292 (1988).
[28] W. D. Heiss and A. A. Kotzé, Phys. Rev. A **44**, 2403 (1991).
[29] J. von Neumann and E. Wigner, Phys. Z. **30**, 467 (1929).
[30] C. E. Zener, Proc. R. Soc. London, Ser. A **137**, 696 (1932).
[31] D. L. Hill and J. A. Wheeler, Phys. Rev. **89**, 1102 (1953).
[32] W. J. Swiatecki, Nucl. Phys. A **488**, 375c (1988).
[33] M. Wilkinson, Phys. Rev. A **41**, 4645 (1990).
[34] D. Kusnezov, in *Symmetries in Science VII*, edited by B. Gruber and T. Otsuka (Plenum Press, New York, 1994).
[35] D. Kusnezov and D. Mitchell, Phys. Rev. C **54**, 147 (1996).
[36] V. Paar, D. Vorkapic, and A. E. L. Dieperink, Phys. Rev. Lett. **69**, 2184 (1992).
[37] A. Bulgac, G. Do Dang, and D. Kusnezov, Phys. Rev. E **54**, 3468 (1996); Phys. Rep. **264**, 67 (1996).
[38] S. Mizutori and S. Åberg, Phys. Rev. E **56**, 6311 (1997).
[39] A. Bulgac, G. Do Dang, and D. Kusnezov, Phys. Rev. E **58**, 196 (1998).